Dalton Transactions

ARTICLE

Dual Oxidase/Oxygenase Reactivity and Resonance Raman Spectra of $\{Cu_3O_2\}$ Moiety with Perfluoro-t-butoxide Ligands

Received 00th January 20xx,
Accepted 00th January 20xx

DOI: 10.1039/x0xx00000x

www.rsc.org/

Sarah E.N. Brazeau[a], Emily E. Norwine[a], Steven F. Hannigan[a], Nicole Orth[b], Ivana Ivanović-Burmazović [b], Dieter Rukser[c], Florian Biebl[c], Benjamin Grimm-Lebsanft[c], Gregor Praedel[c], Melissa Teubner[c], Michael Rübhausen[c], Patricia Liebhäuser[d], Thomas Rösener[d], Julia Stanek[d], Alexander Hoffmann[d], Sonja Herres-Pawlis,*[d] and Linda H. Doerrer*[a]

A Cu(I) fully fluorinated O-donor monodentate alkoxide complex, $K[Cu(OC_4F_9)_2]$, was previously shown to form a trinuclear copper-dioxygen species with a $\{Cu_3(\mu_3\text{-}O)_2\}$ core, $\mathbf{T}_{OC4F9}$, upon reactivity with O_2 at low temperature. Herein is reported a significantly expanded kinetic and mechanistic study of $\mathbf{T}_{OC4F9}$ formation using stopped-flow spectroscopy. The $\mathbf{T}_{OC4F9}$ complex performs catalytic oxidase conversion of hydroquinone to benzoquinone. $\mathbf{T}_{OC4F9}$ also demonstrated hydroxylation of 2,4-di-*tert*-butylphenolate (DBP) to catecholate, making $\mathbf{T}_{OC4F9}$ the first trinuclear species to perform tyrosinase (both monooxygenase and oxidase) chemistry. Resonance Raman spectra were also obtained for $\mathbf{T}_{OC4F9}$, to our knowledge, the first such spectra for any **T** species. The mechanism and substrate reactivity of $\mathbf{T}_{OC4F9}$ are compared to those of its bidentate counter-part, $\mathbf{T}_{pinF}$, formed from $K[Cu(pin^F)(PR_3)]$. The monodentate derivative has both faster initial formation and more diverse substrate reactivity.

[a] *Department of Chemistry, Boston University, 590 Commonwealth Avenue, Boston, MA 02215 (USA); E-mail: doerrer@bu.edu*
[b] *Department Chemie und Pharmazie, Lehrstuhl für Bioanorganische Chemie, Friedrich Alexander Universität Erlangen-Nürnberg, Egerlandstrasse 1, 91058 Erlangen (Germany)*
[c] *Institut für Nanostruktur- und Festkörperphysik, Universität Hamburg, Luruper Chaussee 149, 22761 Hamburg (Germany)*
[d] *Institut für Anorganische Chemie, RWTH Aachen University, Landoltweg 1, 52074 Aachen (Germany); E-mail: sonja.herres-pawlis@ac.rwth-aachen.de*

Electronic Supplementary Information (ESI) available: Additional analytical data, data analysis, substrate product quantification, with respective ^{1}H NMR and MS data. See DOI: 10.1039/x0xx00000x

Introduction

The formation and reactivity of $\{Cu_n\text{-}O_y\}$ moieties are of interest to the scientific community for understanding both industrial and biological oxidation chemistry. We design model systems that attempt to do the same or similar chemistry more efficiently, and lead to better understanding of how systems function,.[1-3] For example, a system that could convert methane to methanol at ambient temperature and pressure is desirable for more sustainable use of this abundant resource. Methane's high C-H bond strength makes this oxidation challenging. Currently for commercial applications, methane is simply combusted, generating a range of products, including CO and CO_2, with limited selectivity, making an alternative pathway desirable.[4] Similarly, benzene is commercially oxidized to phenol via a Friedel-Crafts alkylation with propylene, followed by exposure to O_2. Generation of large quantities of acetone, low yield, and peroxide production make this pathway undesirable.[4, 5]

Investigation of more sophisticated systems seeks to offer alternatives to these expensive and crude oxidation processes. The ideal system will have high turnovers, operate under ambient conditions, and selectively convert reactants to products. Materials that have shown promise in selective hydrocarbon oxidation are zeolites. Unlike either enzymes or small-molecule bioinorganic model complexes, zeolites have an exclusively O-donor, aluminosilicate framework.[6, 7] A well-known and highly characterized zeolite for selective CH_4 oxidation is ZSM-5. The Fe/O loaded ZSM-5, formed by exposure to N_2O, was the first transition metal-based zeolite to selectively catalyze methane to methanol conversion.[8, 9] Fe/O zeolites are highly reactive once formed, but will only oxidize CH_4 in the presence of N_2O.[4]

Cu/O zeolites, on the other hand, are less reactive than Fe/O, but have the advantage of oxidizing methane with the addition of either O_2 or N_2O.[4,10] Cu/O ZSM-5 is able to selectively catalyze methane oxidation at 150 °C. Mechanistic studies on CH_4 oxidation by $\{Cu_2O\}^{2+}$ in ZSM-5 have been done using resonance Raman (rR) spectroscopy and UV-vis.[4, 9, 11-13] Using rR, the catalytic site has been identified as $\{Cu_2O\}^{2+}$, with each Cu coordinated bidentate to the O-donor framework, bridged by an oxido unit.[9] When Cu(I) zeolite is exposed to O_2 under reaction conditions, a $\mu\text{-}\eta^2\text{:}\eta^2$ peroxo-bridged dicopper intermediate is observed before forming $\{Cu_2O\}^{2+}$. This species then oxidizes methane to methanol, regenerating Cu(I) and restarting the cycle.[11]

The related zeolite Cu-MOR is also known to selectively oxidize CH_4 at higher temperatures than ZSM-5 and is believed to have two $\{Cu_2O\}^{2+}$ different active sites.[14] DFT calculations performed on Cu-MOR, suggest that there are two possible reaction routes to $[Cu_2O]^{2+}$ moities. The first path forms two $\{Cu(I)_2(\mu_2\text{-}O)\}$ units via O-O cleavage from a $\{Cu_2O_2\}$ unit reacting with two Cu(I) centers. Along the other path a $\{Cu(II)_2\}$ peroxo-bridged precursor reacts with an {Si-O-Si} unit to form a $\{Si_2O_2\}$ peroxide unit and one $[Cu_2O]^{2+}$ core.[12]

CH_4 activation has also been observed in copper exchanged chabazite (CHA) zeolites, known for reduction of nitrogen oxides, including SSZ-13, SSZ-16, and SSZ-39 and related SAPO-34.[15] More recently, on SSZ-13 and SSZ-39, both trans-μ-1,2-peroxo dicopper(II) and mono-(μ-oxo) dicopper(II) species were spectroscopically identified as active sites.[16] Both of these intermediates are proposed to participate in methane activation.

More recently, there have been efforts to expand the zeolite framework to incorporate greater transition metal nuclearity to test the effect on CH_4 oxidation. In particular, $[Cu_3O_3]^{2+}$ active sites have been reported in both ZSM-5[17, 18] and MOR[19] frameworks. The center is proposed to consist of an alternating Cu and O six-membered ring. [19] CH_4 reactivity by MOR also yielded undesired CO and CO_2.[19] More detailed experimental characterization of zeolite intermediates is still needed to explain this additional reactivity and confirm the proposed structure.[4] Zeolites of greater Cu/O nuclearity have been reported[20] but more in-depth CH_4 oxidation studies are also needed.[4] DFT calculations on formation of $[Cu_3O]$-MOR suggest that a $\{Cu_3O_3\}^{2+}$ core results from side-on O_2 reaction with a $\{Cu_3O\}^{2+}$ unit via a $[\mu\text{-}\eta^2\text{:}\eta^2\text{-peroxo-}Cu^{II}_3O]^{2+}$ intermediate.[12]

While zeolites have shown promise for improved commercial oxidation of methane and related molecules, there are presently few systems that allow us to understand oxidation mechanisms of 3*d* metals in exclusively O-donor environments. Over the years, numerous Cu-O_2 complex systems have been explored to provide understanding of enzyme mechanisms. Virtually all examples involve all N-donor ligand systems to model the histidine-rich biological coordination. The thorough structural and mechanistic investigation of N-donor Cu complexes has allowed for a better understanding of both enzyme structures and the reactions they facilitate. There is a wide array of ligand donor types, including pyridyl[21, 22], imine[23], amine[24-28], pyrazolyl[29-32], and imidazolyl[33, 34] donor groups.

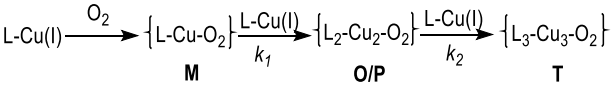

Scheme 1. Stepwise stoichiometric reactivity of Cu(I) with O_2.

The reactivity of Cu(I) with O_2 in both enzymes and model complexes involves step-wise reactivity, with the initial coordination of O_2 to one Cu(I) center, forming a mononuclear species **M**, as shown in Scheme 1, followed by the subsequent addition of a second Cu(I) component. Dinuclear species can have oxo- $\{Cu(III)_2(\mu_2\text{-}O)\}$, **O**, or peroxo containing $\{Cu(II)_2(O_2)\}$, **P**, cores, and are known to exist in equilibrium.[3, 35] Addition of a third Cu(I) reactant can lead to the formation of a trinuclear, **T**, species,[36] which have been reviewed.[1-3, 37] Copper enzyme reactivity with O_2 is controlled by different active sites based on the number of Cu centers and donor ligand environment.[1-3] Examples include mononuclear[38] Cu-containing galactose oxidase,[39, 40] peptidylglycine-α-hydroxylating monooxygenase (PHM),[41] and dopamine-β-monooxygenase (DβM),[41]

dinuclear[42] tyrosinase[43, 44] and catechol oxidase,[45] as well as trinuclear laccase[46] and ascorbate oxidase.[47-49] Particulate methane monooxygenase (pMMO),[50] is proposed to have either one Cu atom and one dinuclear site,[51] or one trinuclear Cu oxide active site in pMMO,.[52, 53]

Some enzymes are highly substrate specific, while others have more flexible reactivity. One such highly specific enzyme is catechol oxidase, which facilitates oxidation of catechols to quinones. On the other hand, tyrosinase[51, 54-60] can perform both the oxidation of catechols to quinones and monooxygenation of phenols to catechols. The dual reactivity of tyrosinase has been the subject of several model complex systems.[24, 25, 31-33, 42-44, 61-72] The design of artifical systems that effect a single type of reactivity and exhibit broad substrate scope remains challenging.

Although many Cu-O_2 studies have involved Cu(I) systems with N-donor ligands, far fewer examples exist with exclusively O-donor systems that could be compared to zeolite systems. In 2013, our group introduced a series of Cu(I) complexes with unique O-donor fluorinated alkoxides that, at low temperatures and in THF, form oxidizing dinuclear and trinuclear Cu_n-O_2 cores.[73] The fully fluorinated complex, $K[Cu(OC_4F_9)_2]$, was evaluated using manometry and determined to have a 3:1 Cu:O_2 ratio, leading to our proposal that the resulting Cu core is a trimer $\{Cu_3(\mu_3\text{-}O)_2\}$, $\mathbf{T_{OC4F9}}$. Two partially fluorinated complexes, $K[Cu(OCMeMe^F{}_2)_2]$ and $K[Cu(OCPhMe^F{}_2)_2]$, have concentration dependent reactivity with O_2, with 2:1 Cu:O_2 species at concentrations below 2 mM, and 3:1 at concentrations above 3 mM. Additionally, when the partially fluorinated species were warmed to RT, intramolecular hydroxylation of sp^2 and sp^3 hybridized C-H bonds, respectively, occurred.[73]

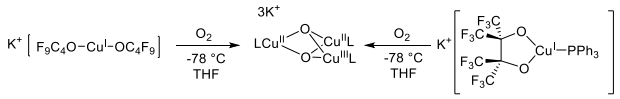

Scheme 2. Formation of $\{Cu_3(\mu_3\text{-}O)_2\}$ from both monodentate and bidentate fluorinated O-donor Cu(I) complexes.

More recently, we reported four cation variants of a fully fluorinated bidentate O-donor complex, $[Cu(pin^F)(PR_3)]^{1-}$, with the perfluoropinacolate (pin^F) ligand.[74] Like its monodentate predecessors, this complex reacts with O_2, forming a symmetric trinuclear species, $^{Sy}\mathbf{T_{pinF}}$ (Scheme 2). $K[Cu(pin^F)(PPh_3)]$ which was fully analyzed kinetically, with the exciting detection of an asymmetric trimer, $^{As}\mathbf{T_{pinF}}$, prior to formation of $^{Sy}\mathbf{T_{pinF}}$. This species, or some rapidly-evolved variant, was also found to catalyze oxidase chemistry in the oxidation of hydroquinone (H_2Q) to benzoquinone (BQ) with a TON of ~ 8.[74]

Herein, we present the full reactivity profile of $K[Cu(OC_4F_9)_2]$, in which we have used a kinetic analysis to detect the initial 1:1 Cu-O_2 intermediate in the formation of the final $\mathbf{T_{OC4F9}}$. The fully fluorinated ligand allows us to achieve both intermolecular substrate oxidase and monooxygenase chemistry, the first for a trinuclear $\{Cu_3O_2\}$ reactive center. The structure is relevant to trinuclear ennnzymes such as laccase and perhaps pMMO, but the reactivity is that of catechol oxidase or tyrosinase. These structural and mechanistic insights offer a molecular Cu O-donor model which may help to understand the reactivity of Cu-loaded zeolites.

Results and Discussion

Characterization of T_{OC4F9}

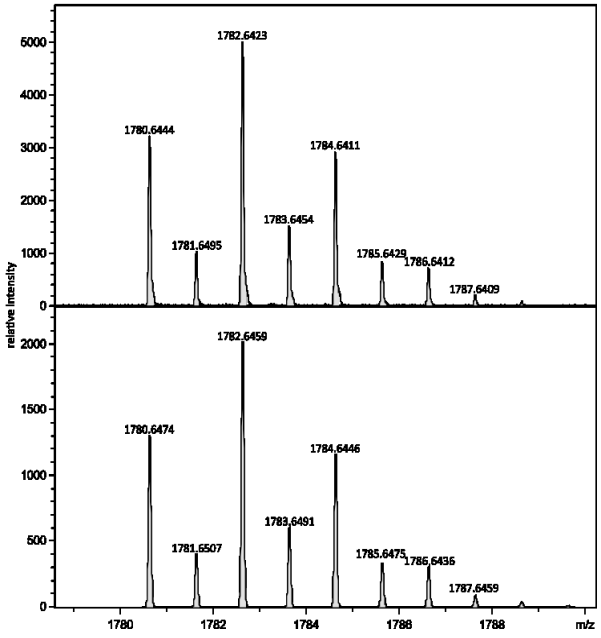

Figure 1. Experimentally observed isotopic pattern for monoanionic $(OC_4F_9)_6Cu^{II}_2Cu^{III}(\mu_3\text{-}O)_2$ $2K^+ + C_4H_8O$ (top) and predicted pattern for $(OC_4F_9)_6Cu^{II}_2Cu^{III}(\mu_3\text{-}O)_2 + 2K^+ + C_4H_8O$ (bottom).

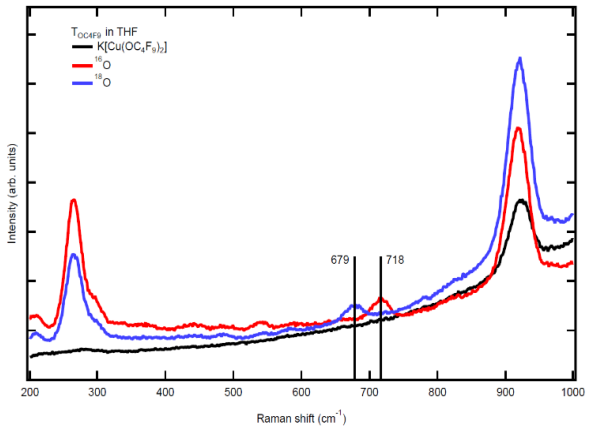

Figure 2. Resonance Raman spectra of T_{OC4F9} showing both ^{16}O (red) and ^{18}O (blue) when [Cu]= 15 mM.

The reactivity of $K[Cu(OC_4F_9)_2]$ and O_2 was previously shown to have a 3:1 Cu:O_2 ratio by manometry.[73] Further evidence of $\{Cu_3(\mu_3\text{-}O)_2\}$ has now been obtained through cryospray-ionization mass spectrometry (CSI-MS) that further confirms this assignment (Figure 1). **T_{OC4F9}** is detected, at 1782.6423 m/z, which includes $(OC_4F_9)_6Cu^{II}_2Cu^{III}(\mu_3\text{-}O)_2$, two K^+ ions, and one equivalent of THF.

We have also recorded the, to our knowledge, first resonance Raman spectrum for a trinuclear, **T**, $\{Cu^{II}_2Cu^{III}(\mu_3\text{-}O_2)\}$ core, as seen in Figure 2 using the excitation wavelength 280 nm. (Spectra collected at other wavelengths are in Figure S1.) Both the ^{16}O and ^{18}O spectra are shown, with features at 718 cm^{-1} and 679 cm^{-1}, respectively, each corresponding to the O···O vector within the trinuclear core. Density functional theory calculations show the expected structure of a **T** core with a localised Cu(III) center and triplet ground state (Figure 3 and Table 1). DFT predicts this vibration to appear in **T** at 652 cm^{-1} with an isotope shift of 34 cm^{-1} to 618 cm^{-1} (TPSSh, GD3BJ/def2-TZVP, SMD THF model, unscaled). A comparable calculation of the singlet ground state (Table 1 and Figure S2) shows an electronic structure higher in energy by 21 kcal/mol. The vibration at 718 cm^{-1} is predicted to originate from O···O stretches involving the (μ_3-O) atoms, as indicated by the shift with the heavier isotope. Importantly, related calculations show that the corresponding vibrations of the related **P** and **O** species would show up at 828 cm^{-1} and 638 cm^{-1}. With regard to the formation characteristics of **T_{OC4F9}** (vide infra), at the

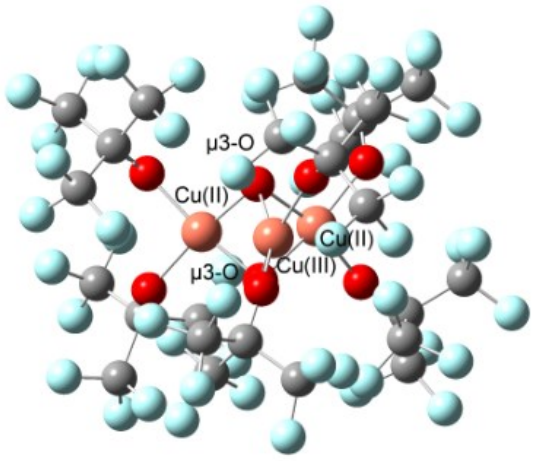

Figure 3. DFT-optimized structure of S = 1 ^{5}**T_{OC4F9}**.

concentrations used for the Raman measurements, only the **T** core is stable in comparison to the **O** core. [1, 75] The resonance Raman spectrum for a related $\{Cu_3S_2\}$ species has been reported with stretches at 367 cm^{-1} and 474 cm^{-1} with ^{32}S that shift to 360 cm^{-1} and 460 cm^{-1} upon labeling with ^{34}S.[76]

The UV-Vis absorption spectrum for **T_{OC4F9}** at -80° C was previously reported, with λ_{max} (ε) values at 307 nm, 520 nm (448), and 602 nm (406).[73] To follow the formation of **T_{OC4F9}** and probe for earlier intermediates, stopped-flow UV-Vis spectroscopy was employed. When solutions of $K[Cu(OC_4F_9)_2]$ and O_2-saturated THF were mixed at -78 °C, the growth of two visible peaks at 520 nm and 602 nm was observed, consistent with previously published data.[73] Peaks corresponding to mononuclear or dinuclear intermediates, such as a bis-μ-oxo core, were not observed before the two visible λ_{max} values slowly grew in, suggesting that any previous intermediates have chromophores similar to **T_{OC4F9}** (Figure 4).[73] Concentrations less than 0.9 mM [Cu^I] were also evaluated

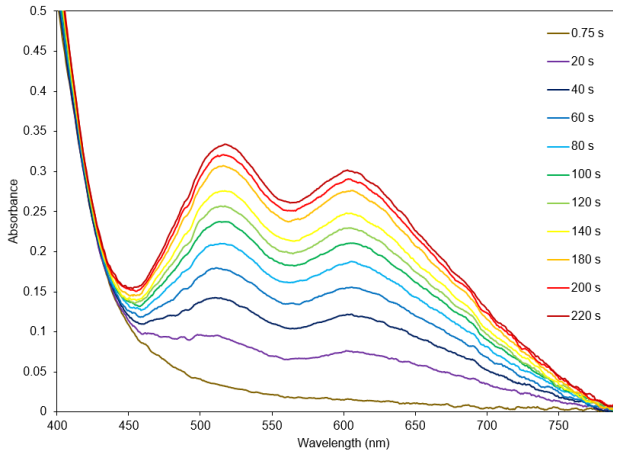

Figure 4. Formation of T_{OC4F9} over 220 s in the visible region, at eleven intervals of 20 s, at 4.95 mM.

due to the high molar absorptivity of the charge transfer band; however, no additional peaks in the UV region were detected. These concentrations proved to be too low to elucidate visible transitions due to small extinction coefficients. We note that any Cu(II) species will have O-to-Cu LMCT from the alkoxide ligands as well as O-to-Cu LMCT from any peroxo or oxo ligands derived from O_2. Therefore, the clear and distinct features attributed to $\{Cu(II)_2(O\text{-}O)\}$ and $\{Cu(III)(\mu_2\text{-}O)\}$ are not expected to be easily distinguishable. Such O-Cu(II) LMCT features were previously reported with a bidentate ligand[77] in $[Cu(pin^F)_2]^{2-}$ (~ 200 – 320 nm) and monodentate perfluoro-t-butoxide[78] in $[Cu(OC_4F_9)_3]^{1-}$ (~ 230 - 400 nm).

Table 1. Calculated bond lengths (Å) of $^{Sy}T_{OC4F9}$.

	***S* = 1 $^{Sy}T_{OC4F9}$**	***S* = 0 $^{Sy}T_{OC4F9}$**
Cu(II)- μ_3-O	1.966- 1.993	1.869 - 1.948
Cu(III)- μ_3-O	1.809- 1.825	1.952
Cu(II)-O_{C4F9}	1.927- 1.954	1.916 - 1.927
Cu(III)-O_{C4F9}	1.895, 1.898	1.960, 1.984
O…O	2.288	2.286
Cu…Cu	2.637- 2.728	2.488- 2.860

Formation of $\mathbf{T_{OC4F9}}$

Stopped-flow kinetic data were evaluated at [Cu^I] ranging from 0.9 mM to 10 mM (Table 2; Figure S3, and Figure S4 in Supporting Information). The data indicate that $\mathbf{T_{OC4F9}}$ forms in a multi-step mechanism. These steps corresponded to (i) an initial species decaying that is proposed to be a rapidly-formed mononuclear {Cu-O_2} species **M**, (ii) the growth and subsequent decay of a second species, proposed to be {Cu_2O_2}, **O/P**, and (iii) growth of a third species {Cu_3O_2}, **T** (Scheme 3). Full analysis and fitting attempts reveal two observable steps, which process is described in detail in the ESI and shown in Figure S5 and Tables S1-4. Tables S1 and S2 depict fits for single wavelength, while Tables S3 and S4 confirm this assignment is consistent with a global analysis. Associated rate constants can be found in Table 2 for each measured concentration. The Cu(I) monodentate alkoxide, K[$Cu(OC_4F_9)_2$], has no absorbance in the visible range and reacts immediately upon exposure to O_2 in the stopped-flow instrument.

Table 2. Formation constants for {Cu_2O_2}, **O**, and {Cu_2O_3}, **T**, cores at different concentrations.

[Cu^I]	k_f of $\mathbf{O_{OC4F9}}$	k_f of $\mathbf{T_{OC4F9}}$
0.90	1.03± 0.14	0.0056± 0.003
2.23	0.98± 0.15	0.0072± 0.003
2.85	0.91± 0.17	0.0095± 0.002
3.97	1.00± 0.25	0.0058± 0.001
4.95	0.90± 0.08	0.0077± 0.003
10.00	0.94± 0.18	0.016± 0.004

The first observable step, the formation of the dinuclear {Cu_2O_2}, is detected via kinetic analysis of the spectral changes in the visible region. Neither the $\mathbf{M_{OC4F9}}$ species nor $\mathbf{O_{OC4F9}}$ are directly spectroscopically observed. The presence of $\mathbf{O_{OC4F9}}$ can be inferred from kinetic fitting of formation of the peak absorbance intensities at 520 nm and 602 nm. Because $\mathbf{T_{OC4F9}}$ grows in with no spectroscopic intermediates, a one-step fit was also evaluated, but is clearly not consistent with the spectroscopic data (Table S2 and Table S4).

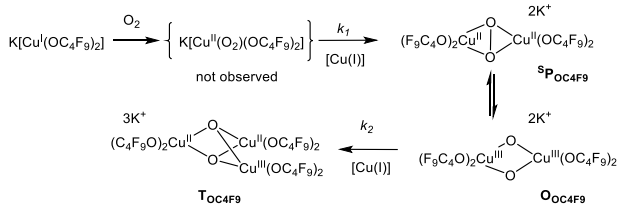

Scheme 3. Proposed mechanism for formation of $\mathbf{T_{OC4F9}}$.

We have assigned this dimer as a {$Cu_2(\mu_2\text{-}O)_2$} **O** core due to the close resemblance of two monodentate OC_4F_9 ligands to the bidentate O-donor pin^F.[74] The proposal of $\mathbf{O_{OC4F9}}$ as a bis-μ-oxo is also based on kinetic and spectroscopic characterization of the recently published K[$Cu(pin^F)(PPh_3)$], a related fluorinated O-donor Cu(I) complex. Upon reactivity of K[$Cu(pin^F)(PPh_3)$] with O_2 at -78 °C, a bis-μ-oxo was detected as a precursor to the final low-temperature stable symmetric trimer.[74] The formation of $\mathbf{O_{OC4F9}}$ could be fit to pseudo-first order conditions in the early stages of the reaction, with a k_f of 0.958± 0.0465 s^{-1}. $\mathbf{O_{OC4F9}}$ is short-lived and begins decaying even before it is fully formed, converting to $\mathbf{T_{OC4F9}}$ as the rate-determining step also under pseudo-first order conditions, with a k_f of 0.00856± 0.00339 s^{-1}. $\mathbf{O_{OC4F9}}$ has a short lifetime, quickly reacting with a third equivalent of Cu(I) alkoxide to form the final proposed product, a symmetric trinuclear core, $\mathbf{T_{OC4F9}}$, whose 3:1 Cu:O_2 ratio was previously confirmed by manometry.[73] Formation of $\mathbf{T_{OC4F9}}$ is the slow step of this mechanism, as confirmed by kinetic analysis of the formation. As confirmed by previous manometry studies, and CSI-MS and resonance Raman herein, the final species is $\mathbf{T_{OC4F9}}$. With increasing reaction time, the growth of $\mathbf{T_{OC4F9}}$ increases more, which is consistent with assigning the third species to the final **T** species. As expected, as [Cu] increases, so does the absorbance at a given reaction time (see Figure S3 for comparison of concentrations at 375 s, and Figure 4 to observe absorbance increase during one-time interval). This trend is not seen with the rate constant, however, as [Cu] and *k* are independent, except for the [Cu] = 14.85 mM case. In this case, [Cu] significantly exceeds [O_2] (10 mM in O_2-saturated THF)[79], and the rate constant becomes dependent on [Cu]. For this example, $k_f(\mathbf{O_{OC4F9}})$ was determined to be 2.1± 0.97 s^{-1}, and $k_f(\mathbf{T_{OC4F9}})$ was determined to be 0.0345± 0.002 s^{-1}.

Because formation of $\mathbf{T_{OC4F9}}$ follows formation of $\mathbf{O_{OC4F9}}$, longer reaction times (75 s and after) provide the most accurate depiction of the $\mathbf{T_{OC4F9}}$ formation kinetic behavior. We propose that this final species is a symmetric trimer, $^{Sy}\mathbf{T_{OC4F9}}$, because no intermediate between the dinuclear and trinuclear species was evident. Since $\mathbf{T_{OC4F9}}$ was found to be stable for at least 3 hours at -78 °C, no k_d was determined (Figure S6). Upon warming to approximately -40 °C, $\mathbf{T_{OC4F9}}$ begins to decay.

$\mathbf{T_{OC4F9}}$ can be directly compared to its fluorinated O-donor and bidentate counter-part, $^{Sy}\mathbf{T_{pinF}}$(Table 3).[74] Both $\mathbf{T_{OC4F9}}$ and $^{Sy}\mathbf{T_{pinF}}$ are the only fully O-donor $\{Cu_3O_2\}^{3-}$ trimers published to date. These systems are alike in forming a trinuclear copper-oxygen core under pseudo first-order conditions upon exposure to THF saturated in O_2 at -78 °C. As shown in Table 3, the initial formation for the dinuclear species with the monodentate ligand, $\mathbf{O_{OC4F9}}$, is faster than $\mathbf{O_{pinF}}$.

The proposed mechanism of $^{Sy}\mathbf{T_{pinF}}$ formation follows the step-wise addition pathway displayed in Scheme 1. The initial conversion is Cu(I) to the monomeric $\mathbf{M_{pinF}}$ (not observed), proposed to be side-on $\mu\text{–}\eta^2\text{:}\eta^2$-peroxodicopper (II) species,

Table 3. Comparison of monodentate-containing $\mathbf{T}_{OC4F9}$ versus bidentate-containing $^{Sy}\mathbf{T}_{pinF}$ formation.

Cu-O_2 Species	λ monitored (nm)	k_f (s^{-1})	reference
$\mathbf{O}_{pinF}$	480	0.418± 0.001	74
$\mathbf{O}_{OC4F9}$	520	0.958± 0.047	This work
$^{Sy}\mathbf{T}_{pinF}$	630	0.268± 0.006	74
$\mathbf{T}_{OC4F9}$	520	0.00856± 0.003	This work

followed by the formation of bis-μ-oxo $\mathbf{O_{pinF}}$. This step can be fit with pseudo-first order kinetics, with a k_f of 0.418± 0.001 s^{-1} (monitored at 480 nm). Formation of $\mathbf{O_{pinF}}$ can be observed at both 380 and 480 nm, which is consistent with formation of the bis-μ-oxo species.[73] As $\mathbf{O_{pinF}}$ decays, the symmetric trimer, $\mathbf{T}_{pinF}$, forms, again fitting with pseudo first-order kinetics with a k_f of 0.268± 0.006 s^{-1}. However, k_d of $\mathbf{O_{pinF}}$ differs from k_f of $\mathbf{T}_{pinF}$, revealing an additional intermediate, $^{As}\mathbf{T_{pinF}}$, before rearrangement to $^{Sy}\mathbf{T_{pinF}}$. The detection of $^{As}\mathbf{T_{pinF}}$ was confirmed by DFT calculations, which showed that $^{As}\mathbf{T_{pinF}}$ was 15.8 kcal/mol higher in energy compared to the symmetric trimer, making the rearrangement to $^{Sy}\mathbf{T_{pinF}}$ thermodynamically favorable.[74] The observation of $^{As}\mathbf{T_{pinF}}$ was significant not just because of its instability, but also because an asymmetric trimer is believed to be an intermediate in the reduction of O_2 to H_2O by multicopper ascorbate oxidase, pMMO, and similar enzymes.[1, 47-49]

Unlike $\mathbf{O_{pinF}}$, which has distinct UV-Vis absorbances that can be monitored for both formation and decay into the final $\mathbf{T_{pinF}}$, $\mathbf{O}_{OC4F9}$ is clearly more reactive, as this intermediate is not distinct spectroscopically. Consistently $^{Sy}\mathbf{T_{pinF}}$ is preceded by $^{As}\mathbf{T}_{pinF}$, and any intermediate $^{As}\mathbf{T_{OC4F9}}$ is not observed in this study. Asymmetric trimers are proposed as precursors to the more common symmetric trimer but are rarely observed[74], therefore the absence of $^{As}\mathbf{T_{OC4F9}}$ in our evaluation is not surprising. $\mathbf{T_{OC4F9}}$ may also go through asymmetric intermediate $^{As}\mathbf{T_{OC4F9}}$ before symmetric trimer formation, but as this process is a subtle rearrangement, it is too fast to observe kinetically.

While several other trimeric systems have been published, to date, only $\mathbf{T_{HPy1MeMe}}$[80] and $^{Sy}\mathbf{T_{pinF}}$[74] have been evaluated kinetically for mechanistic determination. Notably, in formation of $\mathbf{T_{HPy1MeMe}}$, the starting Cu(I) was reacted at low temperature in the presence of O_2 and a mononuclear copper(II)-superoxo intermediate was detected. This formation was fit to pseudo first-order kinetics, with k_{fobs}=0.059 (±0.002) s^{-1}. This is followed by a μ–η^2:η^2-peroxodicopper (II) core which converts to the final **T**.[80]

Substrate Reactivity of T_{OC4F9} vs. $^{SY}T_{pinF}$

To date $^{SY}T_{pinF}$ has only been demonstrated to effect oxidase chemistry.[74] During formation of $^{SY}T_{pinF}$, PPh_3 is oxidized to $O{=}PPh_3$ stoichiometrically, concomitant with loss of the phosphine ligand during trimer formation. Additionally, $^{SY}T_{pinF}$ can catalytically oxidize *para*-hydroquinone (H_2Q) to benzoquinone (BQ). The identity of the phosphine component, PPh_3 or PCy_3, was found to influence the TON slightly, as PPh_3-containing reactants had a TON of 7.85 ± 0.56 with 5 mM [Cu^I] while PCy_3-containing reactants had a TON of 13.87 ± 1.63. The reason for this modest difference is not understood. The presence or absence of 18-crown-6 had little effect on turnover.[74]

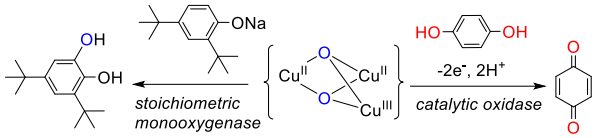

Scheme 4. Dual monooxygenase/oxidase reactivity of T_{OC4F9}.

This successful catalysis led us to investigate T_{OC4F9} under the same conditions. The unique reactivity of T_{OC4F9} is summarized in Scheme 4. Like $^{SY}T_{pinF}$, T_{OC4F9}, or a very closely related species, can catalyze the oxidation of H_2Q to BQ. Using the same conditions as for $^{SY}T_{pinF}$, 10 equivalents of H_2Q were added to the pre-formed trimer. Quantitative ^1H NMR demonstrated the catalytic conversion of H_2Q to BQ, with a turnover of 7. Sieves were added to this reaction in order to raise the TON; however, both the TON and product collection were lower. The T_{OC4F9} core can self-assemble when $K[Cu(OC_4F_9)_2]$ and 10 equivalents of H_2Q are combined, followed by O_2 at low temperatures, yielding similar TONs. (Table S5). Compared to both pin^F systems, the TON for T_{OC4F9} is comparable, slightly higher than that with PPh_3 but less than with the PCy_3 complex (Table 4). This result suggests that the oxidase capacity for each system is similar and the extent of oxidase chemistry is not dependent on whether the ligand is monodentate or bidentate. Interestingly, as revealed by ^1H NMR studies, T_{OC4F9} has other reactivity that accounts for less clean conversion as compared to $^{SY}T_{pinF}$ which has nearly full mass balance observed in product and remaining reactant (Figure S7).[74] As shown in Table 5, the monodentate system forms some product(s) other than BQ, whereas with the bidentate ligand, all the initially-added H_2Q can be accounted for as either unreacted H_2Q or the oxidized BQ. Although this additional reactivity is not understood in detail, we attribute the less selective reactivity of the monodentate complexes, to a more flexible and reactive core that is not permitted with the rigid bidentate pin^F ligand.

Table 4. Catalytic H_2Q oxidation to BQ by T_{OC4F9} in THF at -78° C

Cu^I Source	[Cu^I] (mM)	Cu^I (equiv)	Initial H_2Q (equiv)	Final H_2Q (equiv)	Final BQ (equiv)	TON (per $\{Cu_3O_2\}$ unit)
$K[Cu(OC_4F_9)_2]$	5.0	1.0	10.0 ± 0.0	2.8 ± 1.1	2.6 ± 0.6	7.0 ± 0.5
$K[Cu(PPh_3)(pin^F)]$[74]	5.0	1.0	10.0 ± 0.0	7.1 ± 1.0	2.6 ± 0.2	7.9 ± 0.6
$K[Cu(PCy_3)(pin^F)]$[74]	5.0	1.0	10.0 ± 0.0	4.8 ± 0.4	4.6 ± 0.6	13.9 ± 1.6

Hydroxylation (monooxygenase) reactivity was also investigated with both $^{SY}T_{pinF}$ and T_{OC4F9}, which had not been previously explored with either system. Excitingly, we found that T_{OC4F9} can stoichiometrically hydroxylate 2,4-di-*tert*-butylphenolate (DBP) to 3,5-di-t-butyl-1,2-catechol (DBC). Conditions required for maximum conversion were adding substrate to pre-formed trimer at -78 °C, followed by warming to room temperature and quenching with excess HCl. Quantitative ^1H NMR spectroscopy reveals a TON of 0.91 (Table 5, further details in Table S6). The primary catechol formed is 3,5-di-tert-butylbenzene-1,2-diol (product A in ESI), confirmed with an independent sample, however, 10% of reactions yielded a second catechol, probably 4,6-di-tert-butylbenzene-1,3-diol (product B in ESI). (See Figure S8 where a representative ^1H NMR showing formation of each catechol product can be seen.) Catechol production is also confirmed by DART+ MS, in Figure S9.

In order to confirm that T_{OC4F9} was performing the hydroxylation, ^{18}O labeling experiments were carried out. The 3,5-di-tert-butylbenzene-1,2-catechol was observed via ^1H NMR, shown in Figure S10, and was further confirmed by analysis with DART+ MS (Figure S11), with observation of both labeled and unlabeled catechol.

This heterogeneity can be attributed to similar side reactivity that reduces the yield in the H_2Q oxidation by T_{OC4F9}. We also evaluated $^{SY}T_{pinF}$ under the same reaction conditions; however, no hydroxylation was observed, suggesting that possible core flexibility unique to T_{OC4F9} is required for substrate hydroxylation.

Table 5. Hydroxylation of DBP to catecholate by $\mathbf{T_{OC4F9}}$

[Cu^{I}] (mM)	Cu^{I} (equiv)	Initial Phenolate (equiv)	Final Phenolate (equiv)	Final Catecholate (equiv)	TON (per {Cu_3O_2} unit)
5.0	1.0	1.0 ± 0.0	0.7 ± 0.5	0.1 ± 0.1	0.30
5.0	1.0	5.0 ± 0.0	2.9 ± 0.5	0.3 ± 0.1	0.91

The substrates 4-methoxyphenolate, 2,4-dimethylphenolate, and 8-hydroxyquinolinate were also evaluated under identical conditions, but exhibited no oxygenase or oxidase reactivity with either trimer. No catalytic hydroxylation of DBP to DBC was observed with the addition of 2 equivalents of Et_3N per phenol.

Only a couple examples, to our knowledge, exist of tricopper complexes that can perform C-H activation chemistry with O_2. A related $[Cu^{I}Cu^{I}Cu^{I}(L)]^{+}$ complex, has a mixed N/O donor ligand with eight coordination sites that, when exposed to O_2, forms a presumed bis(μ_3-oxo)$Cu^{II}Cu^{II}Cu^{III}$ moiety[28, 81] that can facilitate both O-atom transfer with benzil and 2,3-butanedione[28], and C-H oxidation of CH_3CN to CH_2OHCN[28], and CH_4 to CH_3OH.[52] Similarly, a Cu_3^{I} cyclophanate that can be oxidized to Cu_3OL has oxidative activity with numerous substrates, including C-H activation of DHA and toluene, and OAT with EtSMe and styrene.[82] Our system is the first **T** species to perform both components of tyrosinase chemistry (oxidase and hydroxylation/monooxygenase) and is the first O-donor system to perform hydroxylation reactivity, with potential relevance for future oxidation studies in O-donor materials.

Other symmetric {$Cu_3(\mu_3\text{-}O)_2$} systems have shown to be able to perform oxidase or O-transfer chemistry. Both $\mathbf{T_{TMCD}}$[36] and $\mathbf{T_{HPy1MeMe}}$[80] perform oxidative coupling of DBP with high yield. Additionally, $\mathbf{T_{\beta\text{-}DKT}}$ facilitates the stoichiometric O-transfer of PPh_3 to $O{=}PPh_3$.[83] The histamine-type ligands in $\mathbf{T_{nBu}}$, $\mathbf{T_{Me2}}$, and $\mathbf{T_{Me3}}$ were investigated for HAT with 5,6-isopropylidene ascorbic acid to compare rates of reactivity between the trimers and the bis-μ-oxo reactive species of the same ligand family.[34]

Most recently, a tris-triamine ligand, structured on a 1,3,5 substituted phenyl, was shown to coordinate three independent Cu(I) atoms tridentate. When this species was exposed to O_2, $[Cu^{II}Cu^{II}(O_2^{3}\text{-})Cu^{II}]$ was formed, through intermediate $[Cu^{I}Cu^{II}(O_2^{2}\text{-})Cu^{II}]$. When the reduced species was combined with O_2, Fc* and TFA, the core was found to catalyze the $4e^{-}/4H^{+}$ reduction of O_2 to H_2O, with TON= 32.[84]

While this reported hydroxylation reactivity by a fully O-donor **T** core is the first, there are many literature examples of side-on {Cu_2O_2} cores performing phenolic hydroxylation chemistry. Many of these are tyrosinase models.[24, 25, 31-34, 43, 44, 61-72] These complex systems feature μ-η^2:η^2-peroxodicopper (II) core to model the active site of tyrosinase, and are able to perform both stoichiometric *o*-phenolate and catalytic *o*-phenol for phenolic substrates with a range of electron donation. A notable recent example presents a μ-η^2:η^2-peroxodicopper (II) core stabilized by three monodentate histidine Nτ-imidazoles, significant due to biological relevance, that can stoichiometrically convert phenolates to catecholates.[63]

There are also examples of arene hydroxylation by bis-μ-oxo centers. A recent example is a bis-μ-oxo supported by tridentate N-donor N-(3-hydroxyphenyl)methyl-bis-(2-picolyl)-amine that oxidizes an attached phenol directly to *ortho*-quinone.[85] Similarly, a bis-μ-oxo featuring a *meta*-xylyl-bridged dinuclear tridentate N-donor ligand can perform the phenol *ortho*-hydroxylation. Notably, the active center was identified as a bis-μ-oxo using resonance Raman spectroscopy during hydroxylation of *p*-chlorophenolate.[62] A bis-μ-oxo complex with 2-(diethylaminoethyl)-6-phenylpyridine bidentate ligands was found to perform hydroxylation of an appending arene, with the products being aldehydes. DFT calculations confirm the bis-μ-oxo as the active center.[86, 87] Lastly, a bis-μ-oxo complex was found to perform intramolecular oxidation of a bridging arene in addition to DBP, yielding C-C coupled dimer, catechol and trace amounts of quinone.[88]

Conclusions

We have now investigated two different O-donor ligand systems in Cu(I)-O_2 reactivity, $\mathbf{T_{OC4F9}}$ and $\mathbf{T_{pinF}}$, enabling us to analyze similarities and differences. $K[Cu(OC_4F_9)_2]$, a monodentate O-donor, fully fluorinated Cu(I) complex, was previously shown to form a reactive $\{Cu_3O_2\}^{3-}$ core, $\mathbf{T_{OC4F9}}$.[73] An expanded kinetic analysis of $\mathbf{T_{OC4F9}}$ provides a proposed mechanism of formation, including a bis-μ-oxo intermediate followed by final symmetric trimer $\mathbf{T_{OC4F9}}$ formation, which is the only directly observable species. Its resonance Raman spectrum was also measured, which is the first measurement for any {Cu_3O_2} **T** species. $\mathbf{T_{OC4F9}}$ is a special {Cu_3O_2} core that can perform both oxidase and oxygenase chemistry. Specifically, $\mathbf{T_{OC4F9}}$ can oxidize H_2Q to BQ catalytically, and DBP to DBC stoichiometrically, confirmed by a labeling experiment with $^{18}O_2$. This dual reactivity is unique to the monodentate ligand system, whereas the related fully fluorinated bidentate ligand system $\mathbf{^{Sy}T_{pinF}}$, only performs H_2Q oxidase chemistry. This difference in reactivity between ligand systems is attributed to the greater flexibility of the monodentate ligand, allowing for a more accessible reactive center. The hydroxylation of DBP to DBC by $\mathbf{T_{OC4F9}}$ is especially noteworthy, as this is one of few trinuclear Cu systems reported to date capable of monooxygenase reactivity. Future studies will involve further kinetic and substrate investigations of similar systems, and increase our understanding of C-H bond oxidation by 3*d* metals in O-donor environments.

Experimental Section

General procedures: Ligand and Cu^{I} complex syntheses were performed as previously described.[74, 89] Cu^{I} complex solutions were prepared at room temperature in an MBraun purified N_2-filled drybox under an inert N_2 atmosphere. The anhydrous solvent tetrahydrofuran (THF) was purified via distillation from sodium benzophenone ketyl under N_2 and degassed. All solvents were stored over molecular sieves in an N_2-filled drybox. ^{18}O (500 mL) was purchased from Sigma Aldrich. ^{1}H-NMR solvents were obtained from Cambridge Scientific. *para*-Hydroquinone and all phenols were obtained from Sigma Aldrich. The subsequent sodium phenolates were synthesized by combining desired phenol and sodium hydride at low temperature, followed by filtration, trituration, and recrystallization. based on a preparation reported in the literature.[62]

Physical Methods: NMR spectra were recorded on a Varian 500 MHz spectrometer at RT. Chemical shifts for ^{1}H were referenced to resonance of residual protiosolvent. UV-Vis data analysis was performed using a Varian Cary 60 spectrophotometer from Agilent Technologies with a fiber-optic quartz glass immersion probe (Hellma, 1 mm) in a customized Schlenk cell. CSI-MS measurements were performed with an ultra-high resolution time-of-flight (UHR-TOF) Bruker Daltonik maXis plus instrument (Bremen, Germany), an ESI-quadrupole time-of-flight (qTOF) mass spectrometer capable of resolution of at least 60.000 at full-width half-maximum (FWHM), which was coupled to a Bruker Daltonik Cryospray unit. Detection was in the negative ion mode and the source voltage was 4.0 kV.The flow rates were 280 $\mu L h^{-1}$. The drying gas (N_2), to aid solvent removal, and the spray gas were held at -90 °C. The machine was calibrated prior to every experiment by direct infusion of the Agilent ESI-TOF low-concentration tuning mixture, which provided an *m/z* range of singly charged peaks up to 28 000 Da in negative ion mode. Stopped-flow spectroscopy experiments were performed with a HI-TECH Scientific SF-61SX2 device with a diode array and photomultiplier detector (Aachen, Germany). The optical light path for transmission of the quartz glass cuvette was 10 mm. The mixing time is given by HITECH as 2 ms. The fastest scan rate was 667 spectra per second in a wavelength range of 250 to 800 nm. The stopped-flow experiments were performed using the TgK Scientific Program Kinetic Studio 4.0.8.18533 (Aachen, Germany). Kinetic analyses were carried out with JPlus Consulting program ReactLab KINETICS (Build 10, Version 1.1). The small dip in absorbance in the first milliseconds of the resulting Absorbance vs. Time plots was due to the viscosity change caused by the release of syringe contents and was removed for more accurate fitting of the experimental data. The resulting spectra, as well as an example of this correction, can be found in the Supporting Information. Resonance Raman (Hamburg, Germany) was performed using a Tsunami Ti:Sapphire laser system model 3960C-15HP (Spectra Physics Lasers Inc., California), used in conjunction with a flexible harmonic generation unit, model GWU2 23-PS (GWU-Lasertechnik Vertriebsges.mbH, Erfstadt) providing the frequency tripled wavelength of 280 nm. To determine the pulse width of the laser, a small part of the Tsunami fundamental was mirrored out using a glass plate and the reflex then coupled into an autocorrelator (AC) (APE GmbH, Berlin, Germany). The laser beam was widened with a spatial filter and then focused on the cuvette inside the cryostat. The focus spot size was around 20 µm in diameter. Raman scattered light was then captured with the entrance optics of the UT-3 triple monochromator spectrometer.[75, 90] The cryostat was a slightly modified version of the previously published method[90] with a standard cuvette with septum instead of PEEK tubes for oxygenation. Equipped with a different Peltier element (QuickCool QC-127-1.4-6.0MS) and a new copper block which encloses three sides of the Suprasil cuvette with a sample volume of 1.4 ml (Hellma Analytics, Müllheim) temperatures below -90 °C inside the solution were reached. The used laser power in front of the entrance optics was ≈3 mW. The pulse width was 1 ps. The experiments were conducted in a clean room with constant temperature (20.0 ˚C ± 0.5 °C) and humidity (45 % ± 3 %). MS measurements were run using Direct Analysis in Real Time (DART) on an AccuTOF time-of-flight (TOF) mass spectrometer (JEOL USA, Inc., Peabody, MA, USA). The resolving power was ~6000 (FWHM definition), measured using Fomblin Y (Sigma Aldrich). Samples were sampled directly by dipping the closed end of a melting point capillary into a sample solution and positioning the sample-coated tube between the DART ion source and the detector inlet. The DART ion source was operated with helium gas (Airgas, Cambridge, MA, USA) at 400oC.

Computational methods: The geometries of the complex anions are fully optimised with density functional theory using the Berny algorithm as implemented in Gaussian 09.[91] The Gaussian 09 calculations are performed with the hybrid functional TPSSh,[92] and with the Ahlrichs type basis set def2-TZVP.[93] We used the SMD model for THF as implemented in Gaussian 09. As empirical dispersion correction, we used the D3 dispersion with Becke–Johnson damping as implemented in Gaussian, Revision D.01.[94, 95] For TPSSh, the values of the original paper have been substituted by the corrected values kindly provided by S. Grimme as private communication. The **P** species was treated as open-shell singlet and a spin expectation value[96] = 0.44 was found. The triplet calculation for the **T** species gave a value for the spin expectation value $\langle S^2 \rangle = 2.00$.

Low temperature UV-Vis spectroscopy: Under inert atmosphere, Cu^{I} complexes were dissolved in THF. The pale yellow solution was transferred to a Hamilton Gastight Syringe. Outside of the drybox, a customized Schlenk measurement cell with a stir bar was sealed with a rubber septum, evacuated and maintained under N_2 atmosphere. A desired volume of THF was added, and O_2 was bubbled in via a balloon and needle for ten minutes. The cell was then cooled to -78 °C using dry ice/acetone. The Cu(I) solution was injected into the cell and evaluated from 200 nm to 800 nm.

Low temperature stopped-flow spectroscopy: Under inert atmosphere, Cu^{I} complexes were dissolved in THF. The pale

yellow solution was then transferred to a Hamilton Gastight Syringe. Outside of the drybox, dioxygen was bubbled from a balloon into previously distilled and degassed THF to saturate the solution. The O_2-saturated THF (10 mM)[79] was then transferred into a second Hamilton Gastight Syringe. The two syringes were connected to the stopped-flow spectrometer for evaluation at -78 °C.

Low temperature resonance Raman: The complex was prepared in an oxygen and water free atmosphere (< 0.5 ppm) inside a LABstar glovebox (MBraun, Garching) with a concentration of ≈15 mM (based on Cu(I) precursor) in 99.9 % THF (VWR Chemicals, Pennsylvania). The solvent was degassed and dried over sodium. Additional drying over a 3 Å molecular sieve was necessary before measuring. After cooling the precursor solution to below -90 °C, oxygen was run through the sample using cannulas for ≈10 mins until the complex was formed. This can be observed by a distinct change in color of the solution from slightly yellow to deep purple. The cryostat was then placed inside the entrance optics of the UT-3 Raman spectrometer. With a micrometer screw a focal depth of around 50 µm inside the cuvette was adjusted.

Catalytic conversion of H_2Q: The conversion of H_2Q to BQ by $\mathbf{T_{OC4F9}}$ was performed as previously reported for $^{Sy}\mathbf{Tpin^F}$.[74] In the drybox, Cu^I complexes were dissolved in THF in a Schlenk flask, and transferred to the Schlenk line under N_2 atmosphere. The solution was cooled to -78 °C using a dry ice/acetone bath, and then O_2 bubbled into the solution from a balloon fitted with a needle and syringe, affording a royal purple solution. Following trimer formation, the solution was purged with N_2 for ten minutes. In the glovebox, 10 equivalents of H_2Q were measured out and dissolved in 1 mL THF, and sealed in a vial with a septum. The substrate was added to the complex solution, under a positive pressure of N_2, resulting in a maroon-brown solution. The solution was stirred at -78 °C for 30 minutes, and then allowed to warm up to RT. The solution was then concentrated, and the resulting residue was dissolved in d_6-acetone and evaluated by ^{1}H NMR spectroscopy. Both starting material and products were quantified using an internal standard of DMSO. See Table S5 for calculation of H_2Q and BQ yields.

Stoichiometric reactions with 2,4-DBP: In the drybox, Cu^I complexes were dissolved in THF in a Schlenk flask and transferred to the Schlenk line under N_2 atmosphere. The solution was cooled to -78 °C using dry ice/acetone, and then O_2 bubbled into the solution from a balloon fitted with a needle and syringe, affording a royal purple solution. Following trimer formation, the solution was purged with N_2 for ten minutes. In the glovebox, 5 equivalents of 2,4-DBP were measured out and dissolved in 0.5 mL THF, and sealed in a vial with a septum. The substrate was transferred to the complex solution, under a positive pressure of N_2, and resulting in an olive green solution. The solution was stirred at -78 °C for 10 minutes, turning slightly more yellow, warmed up to RT and stirred for 30 minutes, and quenched with 3 mL of 0.5 M HCl. The solution was partially concentrated to remove THF, followed by three extractions into DCM. The organic layer was concentrated to a yellow oil which was then dissolved in CD_2Cl_2. Acetophenone was added as an internal standard prior to analysis by ^{1}H NMR spectroscopy. Using the internal standard, both starting material and products were quantified. See Table S6 for calculation of phenol and catechol yields.

Stoichiometric reaction with 2,4-DBP and ^{18}O: In the drybox, Cu^I complexes were dissolved in THF in a Schlenk flask and transferred to the Schlenk line, and left sealed. The solution was cooled to -78 °C using dry ice/acetone to create a vacuum. A small balloon was purged with N_2, fully evacuated, and then filled with ^{18}O. The balloon was attached to a needle and then submerged into the solution for one-two minutes, until no longer bubbling. The needle was then raised above the solution, and the reaction proceeded in a sealed environment for 30 minutes. Following trimer formation, the solution was purged with N_2 for ten minutes. In the glovebox, 5 equivalents of 2,4-DBP were measured out and dissolved in 0.5 mL THF, and sealed in a vial with a septum. The substrate was transferred to the complex solution, under a positive pressure of N_2, and resulting in an olive green solution. The solution was stirred at -78 °C for 10 minutes, turning slightly more yellow, warmed up to RT and stirred for 30 minutes, and quenched with 3 mL of 0.5 M HCl. The solution was partially concentrated to remove THF, followed by three extractions into DCM. The organic layer was concentrated to a yellow oil which was then dissolved in CD_2Cl_2. Acetophenone was added as an internal standard prior to analysis by ^{1}H NMR spectroscopy.

Conflicts of interest

There are no conflicts to declare.

Acknowledgements

We gratefully acknowledge the financial support of NSF CHE 0619339 (NMR spectrometer at Boston University), NSF CHE CAT 1800313 (L.H.D), NSF SusChEM 01362550 (L.H.D.), Boston University UROP (E.E.N.), the Deutsche Forschungsgemeinschaft (S. H.-P.: SPP1740 (HE5480/10-1) and SeleCa), (S.H.P. and M.R.: FOR1405), and the "Solar Technologies Go Hybrid" initiative of the State of Bavaria (I.I.-B. and N.O.) for their support. T.R. thanks the Fonds der Chemischen Industrie for granting a Fonds fellowship. We thank Marek Domin (Boston College) for DART MS analysis.

Dalton Transactions

ARTICLE

Notes and references

1. C. E. Elwell, N. L. Gagnon, B. D. Neisen, D. Dhar, A. D. Spaeth, G. M. Yee and W. B. Tolman, *Chem. Rev.*, 2017, **117**, 2059-2107.
2. E. A. Lewis and W. B. Tolman, *Chem. Rev.*, 2004, **104**, 1047-1076.
3. L. M. Mirica, X. Ottenwaelder and T. D. P. Stack, *Chem. Rev.*, 2004, **104**, 1013-1045.
4. B. E. R. Snyder, M. L. Bols, R. A. Schoonheydt, B. F. Sels and E. I. Solomon, *Chem. Rev.*, 2018, **118**, 2718-2768.
5. B. Liptáková, M. Báhidský and M. Hronec, *Applied Catalysis A: General*, 2004, **263**, 33-38.
6. C. S. Cundy and P. A. Cox, *Chem. Rev.*, 2003, **103**, 663-702.
7. T. Ikuno, J. Zheng, A. Vjunov, M. Sanchez-Sanchez, M. A. Ortuño, D. R. Pahls, J. L. Fulton, D. M. Camaioni, Z. Li, D. Ray, B. L. Mehdi, N. D. Browning, O. K. Farha, J. T. Hupp, C. J. Cramer, L. Gagliardi and J. A. Lercher, *J. Am. Chem. Soc.*, 2017, **139**, 10294-10301.
8. G. I. Pannov, V. I. Sobolev and A. S. Kharitonov, *J. Mol. Catal.*, 1990, **61**, 85-97.
9. J. S. Woertink, P. J. Smeets, M. H. Groothaert, M. A. Vance, B. F. Sels, R. A. Schoonheydt and E. I. Solomon, *Proc. Natl. Acad. Sci. USA*, 2009, **106**, 18908-18913.
10. E. Borfecchia, P. Beato, S. Svelle, U. Olsbye, C. Lamberti and S. Bordiga, *Chem. Soc. Rev.*, 2018, **47**, 8097-8133.
11. P. J. Smeets, R. G. Hadt, J. S. Woertink, P. Vanelderen, R. A. Schoonheydt, B. F. Sels and E. I. Solomon, *J. Am. Chem. Soc.*, 2010, **132**, 14736-14738.
12. M. H. Mahyuddin, T. Tanaka, A. Staykov, Y. Shiota and K. Yoshizawa, *Inorg. Chem.*, 2018, **57**, 10146-10152.
13. M. H. Mahyuddin, Y. Shiota, A. Staykov and K. Yoshizawa, *Acc. Chem. Res.*, 2018, **51**, 2382-2390.
14. P. Vanelderen, B. E. R. Snyder, M.-L. Tsai, R. G. Hadt, J. Vancauwenbergh, O. Coussens, R. A. Schoonheydt, B. F. Sels and E. I. Solomon, *J. Am. Chem. Soc.*, 2015, **137**, 6383-6392.
15. M. J. Wulfers, S. Teketel, B. Ipek and R. F. Lobo, *Chem. Commun.*, 2015, **51**, 4447-4450.
16. B. Ipek, M. J. Wulfers, H. Kim, F. Göltl, I. Hermans, J. P. Smith, K. S. Booksh, C. M. Brown and R. F. Lobo, *ACS Catalysis*, 2017, **7**, 4291-4303.
17. G. Li, P. Vassilev, M. Sanchez-Sanchez, J. A. Lercher, E. J. M. Hensen and E. A. Pidko, *J. Catal.*, 2016, **338**, 305-312.
18. M. A. C. Markovits, A. Jentys, M. Tromp, M. Sanchez-Sanchez and J. A. Lercher, *Top. Catal.*, 2016, **59**, 1554-1563.
19. S. Grundner, M. A. C. Markovits, G. Li, M. Tromp, E. A. Pidko, E. J. M. Hensen, A. Jentys, M. Sanchez-Sanchez and J. A. Lercher, *Nat. Comm.*, 2015, **6**, 7546.
20. T. Patrick, M. Ali, B. S. E., K. Frank, P. M. Bum, A. E. M. C., R. Marco and v. B. J. A., *Angew. Chem. Int. Ed.*, 2016, **55**, 5467-5471.
21. S. Kim, J. Y. Lee, R. E. Cowley, J. W. Ginsbach, M. A. Siegler, E. I. Solomon and K. D. Karlin, *J. Am. Chem. Soc.*, 2015, **137**, 2796-2799.
22. J. Y. Lee, R. L. Peterson, K. Ohkubo, I. Garcia-Bosch, R. A. Himes, J. Woertink, C. D. Moore, E. I. Solomon, S. Fukuzumi and K. D. Karlin, *J. Am. Chem. Soc.*, 2014, **136**, 9925-9937.
23. S. Hong, L. M. Hill, A. K. Gupta, B. D. Naab, J. B. Gilroy, R. G. Hicks, C. J. Cramer and W. B. Tolman, *Inorg. Chem.*, 2009, **48**, 4514-4523.
24. K. V. N. Esguerra, Y. Fall and J.-P. Lumb, *Angew. Chem. Int. Ed.*, 2014, **53**, 5877-5881.
25. K. V. N. Esguerra, Y. Fall, L. Petitjean and J.-P. Lumb, *J. Am. Chem. Soc.*, 2014, **136**, 7662-7668.
26. S. Itoh, *Acc. Chem. Res.*, 2015, **48**, 2066-2074.
27. A. Kunishita, M. Kubo, H. Sugimoto, T. Ogura, K. Sato, T. Takui and S. Itoh, *J. Am. Chem. Soc.*, 2009, **131**, 2788-2789.
28. P. P.-Y. Chen, R. B.-G. Yang, J. C.-M. Lee and S. I. Chan, *Proc. Natl. Acad. Sci. USA*, 2007, **104**, 14570-14575.
29. K. Fujisawa, *J. Biol. Inorg. Chem.*, 2017, **22**, 237-251.
30. N. Kitajima, K. Fujisawa, C. Fujimoto, Y. Morooka, S. Hashimoto, T. Kitagawa, K. Toriumi, K. Tatsumi and A. Nakamura, *J. Am. Chem. Soc.*, 1992, **114**, 1277-1291.
31. J. N. Hamann and F. Tuczek, *Chem. Commun.*, 2014, **50**, 2298-2300.
32. P. Liebhäuser, K. Keisers, A. Hoffmann, T. Schnappinger, I. Sommer, A. Thoma, C. Wilfer, R. Schoch, K. Stührenberg, M. Bauer, M. Dürr, I. Ivanović-Burmazović and S. Herres-Pawlis, *Chem. Eur. J.*, 2017, **23**, 12171-12183.
33. S. Palavicini, A. Granata, E. Monzani and L. Casella, *J. Am. Chem. Soc.*, 2005, **127**, 18031-18036.
34. J. B. Gary, C. Citek, T. A. Brown, R. N. Zare, E. C. Wasinger and T. D. P. Stack, *J. Am. Chem. Soc.*, 2016, **138**, 9986-9995.
35. J. A. Halfen, S. Mahapatra, E. C. Wilkinson, S. Kaderli, V. G. Young, L. Que, A. D. Zuberbühler and W. B. Tolman, *Science*, 1996, **271**, 1397-1400.
36. A. P. Cole, D. E. Root, P. Mukherjee, E. I. Solomon and T. D. P. Stack, *Science*, 1996, **273**, 1848-1850.
37. E. Salvadeo, L. Dubois and J.-M. Latour, *Coord. Chem. Rev.*, 2018, **374**, 345-375.
38. S. Itoh, *Acc. Chem. Res.*, 2015, **48**, 2066-2074.
39. B. A. Jazdzewski and W. B. Tolman, *Coord. Chem. Rev.*, 2000, **200-202**, 633-685.
40. D. Yin, S. Urresti, M. Lafond, E. M. Johnston, F. Derikvand, L. Ciano, J.-G. Berrin, B. Henrissat, P. H. Walton, G. J. Davies and H. Brumer, *Nat. Comm.*, 2015, **6**, 10197.
41. B. F. Gherman, D. E. Heppner, W. B. Tolman and C. J. Cramer, *J. Biol. Inorg. Chem.*, 2006, **11**, 197-205.

42. F. Wendt, C. Naether and F. Tuczek, *J. Biol. Inorg. Chem.*, 2016, **21**, 777-792.
43. P. Liebhäuser, A. Hoffmann and S. Herres-Pawlis, in *Reference Module in Chemistry, Molecular Sciences and Chemical Engineering*, Elsevier, 2016, DOI: https://doi.org/10.1016/B978-0-12-409547-2.11554-9.
44. J. N. Hamann, B. Herzigkeit, R. Jurgeleit and F. Tuczek, *Coord. Chem. Rev.*, 2017, **334**, 54-66.
45. I. A. Koval, P. Gamez, C. Belle, K. Selmeczi and J. Reedijk, *Chem. Soc. Rev.*, 2006, **35**, 814-840.
46. L. M. Mirica and T. D. P. Stack, *Inorg. Chem.*, 2005, **44**, 2131-2133.
47. E. I. Solomon, *Inorg. Chem.*, 2016, **55**, 6364-6375.
48. J. Yoon and E. I. Solomon, *J. Am. Chem. Soc.*, 2007, **129**, 13127-13136.
49. A. Messerschmidt, A. Rossi, R. Ladenstein, R. Huber, M. Bolognesi, G. Gatti, A. Marchesini, R. Petruzzelli and A. Finazzi-Agró, *J. Mol. Biol.*, 1989, **206**, 513-529.
50. V. C. C. Wang, S. Maji, P. P. Y. Chen, H. K. Lee, S. S. F. Yu and S. I. Chan, *Chem. Rev.*, 2017, **117**, 8574-8621.
51. R. L. Peterson, S. Kim and K. D. Karlin, in *Comprehensive Inorganic Chemistry II (Second Edition)*, ed. K. Poeppelmeier, Elsevier, Amsterdam, 2013, DOI: https://doi.org/10.1016/B978-0-08-097774-4.00309-0, pp. 149-177.
52. S. I. Chan, Y.-J. Lu, P. Nagababu, S. Maji, M.-C. Hung, M. M. Lee, I.-J. Hsu, P. D. Minh, J. C.-H. Lai, K. Y. Ng, S. Ramalingam, S. S.-F. Yu and M. K. Chan, *Angew. Chem. Int. Ed.*, 2013, **52**, 3731-3735.
53. S. I. Chan, K. H. C. Chen, S. S. F. Yu, C.-L. Chen and S. S. J. Kuo, *Biochemistry*, 2004, **43**, 4421-4430.
54. S. Itoh and S. Fukuzumi, *Acc. Chem. Res.*, 2007, **40**, 592-600.
55. A. Bijelic, M. Pretzler, C. Molitor, F. Zekiri and A. Rompel, *Angew. Chem.*, 2015, **127**, 14889-14893.
56. A. Bijelic, M. Pretzler, C. Molitor, F. Zekiri and A. Rompel, *Angew. Chem. Int. Ed.*, 2015, **54**, 14677-14680.
57. C. M. S.G. Mauracher, R. Al-Oweini, U. Kortz, A. Rompel,, *Acta Cryst.*, 2014, **D70**, 2301- 2315.
58. J. L. Muñoz-Muñoz, J. Berna, M. d. M. García-Molina, F. Garcia-Molina, P. A. Garcia-Ruiz, R. Varon, J. N. Rodriguez-Lopez and F. Garcia-Canovas, *Biochem. Biophys. Res. Commun.*, 2012, **424**, 228-233.
59. S.-i. Yamazaki and S. Itoh, *J. Am. Chem. Soc.*, 2003, **125**, 13034-13035.
60. E. Solem, F. Tuczek and H. Decker, *Angew. Chem., Int. Ed.*, 2016, **55**, 2884-2888.
61. M. Rolff, J. Schottenheim, H. Decker and F. Tuczek, *Chem. Soc. Rev.*, 2011, **40**, 4077-4098.
62. A. Company, S. Palavicini, I. Garcia-Bosch, R. Mas-Ballesté, L. Que, E. V. Rybak-Akimova, L. Casella, X. Ribas and M. Costas, *Chem. Eur. J.*, 2008, **14**, 3535-3538.
63. L. Chiang, W. Keown, C. Citek, E. C. Wasinger and T. D. P. Stack, *Angew. Chem., Int. Ed.*, 2016, **55**, 10453-10457.
64. C. Citek, C. T. Lyons, E. C. Wasinger and T. D. P. Stack, *Nat. Chem.*, 2012, **4**, 317-322.
65. A. Hoffmann, C. Citek, S. Binder, A. Goos, M. Ruebhausen, O. Troeppner, I. Ivanovic-Burmazovic, E. C. Wasinger, T. D. P. Stack and S. Herres-Pawlis, *Angew. Chem., Int. Ed.*, 2013, **52**, 5398-5401.
66. M. Rolff, J. Schottenheim, G. Peters and F. Tuczek, *Angew. Chem. Int. Ed.*, 2010, **49**, 6438-6442.
67. O. Sander, A. Henß, C. Näther, C. Würtele, M. C. Holthausen, S. Schindler and F. Tuczek, *Chem. Eur. J.*, 2008, **14**, 9714-9729.
68. C. Wilfer, P. Liebhäuser, A. Hoffmann, H. Erdmann, O. Grossmann, L. Runtsch, E. Paffenholz, R. Schepper, R. Dick, M. Bauer, M. Dürr, I. Ivanović-Burmazović and S. Herres-Pawlis, *Chem. Eur. J.*, 2015, **21**, 17639-17649.
69. M. Reglier, C. Jorand and B. Waegell, *J. Chem. Soc., Chem. Commun.*, 1990, DOI: 10.1039/C39900001752, 1752-1755.
70. Z. Huang, M. S. Askari, K. V. N. Esguerra, T.-Y. Dai, O. Kwon, X. Ottenwaelder and J.-P. Lumb, *Chem. Sci.*, 2016, **7**, 358-369.
71. M. S. Askari, K. V. N. Esguerra, J.-P. Lumb and X. Ottenwaelder, *Inorg. Chem.*, 2015, **54**, 8665-8672.
72. L. M. Sayre and D. V. Nadkarni, *J. Am. Chem. Soc.*, 1994, **116**, 3157-3158.
73. J. S. Lum, L. Tahsini, J. A. Golen, C. Moore, A. L. Rheingold and L. H. Doerrer, *Chem. Eur. J.*, 2013, **19**, 6374-6384.
74. S. F. Hannigan, A. I. Arnoff, S. E. Neville, J. S. Lum, J. A. Golen, A. L. Rheingold, N. Orth, I. Ivanović-Burmazović, P. Liebhäuser, T. Rösener, J. Stanek, A. Hoffmann, S. Herres-Pawlis and L. H. Doerrer, *Chem. Eur. J.*, 2017, **23**, 8212-8224.
75. B. Grimm-Lebsanft, C. Brett, F. Strassl, D. Rukser, M. Biednov, F. Biebl, M. Naumova, A. Hoffmann, L. Akinsinde, D. Brueckner, S. Herres-Pawlis and M. Ruebhausen, *Inorg. Chim. Acta*, 2017, **481**, 176- 180.
76. E. C. Brown, J. T. York, W. E. Antholine, E. Ruiz, S. Alvarez and W. B. Tolman, *J. Am. Chem. Soc.*, 2005, **127**, 13752-13753.
77. L. Tahsini, S. E. Specht, J. S. Lum, J. J. M. Nelson, A. F. Long, J. A. Golen, A. L. Rheingold and L. H. Doerrer, *Inorg. Chem.*, 2013, **52**, 14050-14063.
78. S. A. Cantalupo, J. S. Lum, M. C. Buzzeo, C. Moore, A. G. Di Pasquale, A. L. Rheingold and L. H. Doerrer, *Dalton Trans.*, 2010, **39**, 374-383.
79. J. A. E. Gladysz, C., in *Handbook of Fluorous Chemistry*, ed. J. A. C. Gladysz, D.P.; Horvath, I.T., Wiley-VCH, Weinheim, Germany, 2004, pp. 17- 18.
80. M. Taki, S. Teramae, S. Nagatomo, Y. Tachi, T. Kitagawa, S. Itoh and S. Fukuzumi, *J. Am. Chem. Soc.*, 2002, **124**, 6367-6377.
81. S. Maji, J. C.-M. Lee, Y.-J. Lu, C.-L. Chen, M.-C. Hung, P. P.-Y. Chen, S. S.-F. Yu and S. I. Chan, *Chem. Eur. J.*, 2012, **18**, 3955-3968.
82. B. J. Cook, G. N. Di Francesco, M. T. Kieber-Emmons and L. J. Murray, *Inorg. Chem.*, 2018, **57**, 11361-11368.
83. A. K. Gupta and W. B. Tolman, *Inorg. Chem.*, 2012, **51**, 1881-1888.
84. X. Engelmann, E. R. Farquhar, J. England and K. Ray, *Inorg. Chim. Acta*, 2018, **481**, 159-165.
85. J. N. Hamann, M. Rolff and F. Tuczek, *Dalton Trans.*, 2015, **44**, 3251-3258.
86. J. Becker, P. Gupta, F. Angersbach, F. Tuczek, C. Näther, M. C. Holthausen and S. Schindler, *Chem. Eur. J.*, 2015, **21**, 11735-11744.
87. P. L. Holland, K. R. Rodgers and W. B. Tolman, *Angew. Chem., Int. Ed.*, 1999, **38**, 1139-1142.
88. S. Mandal, J. Mukherjee, F. Lloret and R. Mukherjee, *Inorg. Chem.*, 2012, **51**, 13148-13161.

89. S. F. Hannigan, J. S. Lum, J. W. Bacon, C. Moore, J. A. Golen, A. L. Rheingold and L. H. Doerrer, *Organometallics*, 2013, **32**, 3429-3436.
90. B. Schulz, J. Bäckström, D. Budelmann, R. Maeser, M. Rübhausen, M. V. Klein, E. Schoeffel, A. Mihill and S. Yoon, *Rev. Sci. Instrum.*, 2005, **76**, 073107.
91. M. J. Frisch, Gaussian, Inc., Wallingford, CT, **2009**.
92. J. Tao, J. P. Perdew, V. N. Staroverov and G. E. Scuseria, *Phys. Rev. Lett.*, 2003, **91**, 146401.
93. F. Weigend and R. Ahlrichs, *Phys. Chem. Chem. Phys.*, 2005, **7**, 3297-3305.
94. L. Goerigk and S. Grimme, *Phys. Chem. Chem. Phys.*, 2011, **13**, 6670-6688.
95. S. Grimme, S. Ehrlich and L. Goerigk, *J. Comput. Chem.*, 2011, **32**, 1456-1465.
96. A. Bell-Taylor, J. D. Gorden, E. E. Hardy and C. R. Goldsmith, *Inorg. Chim. Acta*, 2018, **482**, 206-212.